# A viscoelastic-viscoplastic model with non associative plasticity for the modelling of bonded joints at high strain rates

Ludovic Dufour, Benjamin Bourel, Franck Lauro, Grégory Haugou, Nicolas Leconte

International Journal of Adhesion & Adhesives 70 (2016) 304–314

# A viscoelastic-viscoplastic model with non associative plasticity for the modelling of bonded joints at high strain rates

Ludovic Dufour [1], Benjamin Bourel, Franck Lauro [1], Gregory Haugou, Nicolas Leconte
1 University of Valenciennes and Hainaut Cambrésis, LAMIH, UMR CNRS 8201, F-59313 Valenciennes, France
E-mail addresses: ludovic.dufour@univ-valenciennes.fr (L. Dufour), franck.lauro@univ-valenciennes.fr (F. Lauro).

## ABSTRACT

The purpose of this work is to present a constitutive model able to represent the behaviour of rubber-toughened adhesive joints under dynamic loading. A fully coupled viscoelastic–viscoplastic damage model at finite strains developed for mineral filled semi-crystalline polymer is identified for an epoxy adhesive. The parameters of the model are identified from experimental tests undertaken on bulk material in compression and tension at several loading speeds. In order to validate the accuracy of the model to represent bonded joints, a specific dynamic Arcan device is used. Experimental tests on this apparatus are carried out for tensile, shear and mixed tensile/shear loadings at 1 mm/s, 10 mm/s and 100 mm/s. A very good agreement between experimental and numerical results is obtained for a large strain rate range and for various stress states.

*Keywords:*
Adhesive bonding
Viscoplasticity
Bulk adhesive
Arcan test

## 1. Introduction

The use of adhesive-bonding is becoming increasingly common in the automotive industry, which aims at improving structural performance and reducing the vehicle weight. Recently, a new generation of adhesives (toughened adhesives) has been developed in order to enhance the ductility of adhesives used in vehicle bodies and to improve their performance under dynamic loadings. The matrix of epoxy-based adhesives in particular is modified by addition of nodules affecting plasticity and other mechanical properties such as viscoelasticity, viscoplasticity and damage evolution during plasticity [8,15]. This leads to more complex adhesives, which increases the difficulties of modelling, particularly, for vehicle crashworthiness analysis.

Various methods are used to model the adhesive joint. The first one is based on a discrete approach which consists in using cohesive elements [19,26]. The second one is a continuous approach based on the use of standard finite elements with a fine description of the constitutive law. An overview of adhesive-bond modelling in crash simulations with a comparison between the continuum elements and the cohesive ones is given in [10].

With the continuum approach, the stress-strain relation for adhesive materials shows similar characteristics as that observed in the inelastic behaviour of polymers. The elasto-plastic (or visco-plastic) material models based on continuum theories or micro-mechanisms are generally used. Classical elasto-plastic models with pressure-independent yield conditions (eg. von Mises) are widely available in commercial codes and widely used since they require a low number of input parameters [25]. However, these criteria cannot accurately predict the behaviour of adhesives under multiaxial loading, as yielding in these materials is sensitive to hydrostatic as well as deviatoric stresses [22]. As a consequence, pressure-dependent plasticity theory is more appropriate in this case. In this context, the Drucker-Prager yield criterion is widely used for polymeric materials [18]. In addition, the mechanical properties of polymers, including structural adhesives, are generally sensitive to the strain rate [4,15]. The effect of the strain rate sensitivity on the behaviour of bulk materials of epoxy resin adhesives is analysed in [14]. It leads to complex behaviours which could be described by different models as non-linear viscoelasticity [1], viscoplasticity [21], coupled elasto-viscoplasticity [9,16], viscoelasticity–viscoplasticity [11].

Two kinds of tests are generally used for the mechanical characterisation of adhesive. The first kind is achieved on bulk adhesive specimens [15,18]. It leads to a direct identification of the stress/strain relation. These tests are only limited by the difficulty to obtain pore-free samples due to the original packaging of the adhesive. The strain-rate effect can be determined by using digital image correlation technique (DIC) [17]. The second kind of test is achieved on assemblies. It permits a characterisation of bonded joints in conditions close to those used in industry, with a thin adhesive layer. But these experiments suffer from a global response highly sensitive to the adherent properties. Moreover, high stress

DOI : 10.1016/j.ijadhadh.2016.07.015

heterogeneities near the edge of the joint do not allow to directly obtain the constitutive law and a reverse identification is often necessary. Some works deal with the reduction of the edge effect by the use of a special Arcan testing device in quasi-static [5] and in dynamic [7] loading conditions. The final objective of all these works is to determine the failure occurrence of the joint. The knowledge of the stress state into the joint is then mandatory. The model generally used or experiments often limit this knowledge.

The objective of this paper is to focus on the identification and modelling of the SikaPower498 adhesive behaviour under multi-axial loadings for a large strain rate range ($0.1\ s^{-1}$ up to $500\ s^{-1}$). To reach this objective, specific dynamic tests have been performed, first, on bulk specimen associated to an original approach with digital image correlation analysis, and secondly, with a new Arcan device especially designed to reach high strain rates into the joint.

Concerning the modelling, the complex behaviour of the adhesive is taken into account by using a viscoelastic–viscoplastic model which is an extension of the elasto-viscoplastic model proposed for polymer by Balieu [2,3].

## 2. Constitutive model description

### 2.1. Viscoelasticity

The viscoelastic model is coupled with a viscoplastic model to take the strain rate sensitivity into account at an early stage of the deformation process. The behaviour of the material is based on the assumption that the rate of deformation $D^t$ is divided into viscoelastic and viscoplastic parts such as :

$$D^t = D^{ve} + D^{vp} \tag{1}$$

This decomposition of the rate of deformation is linked to the hypoelastic formulation which requires for large deformations to achieve incremental objectivity in order to ensure material frame indifference during large deformations/rotations [2]. The linear Wiechert viscoelastic model is used in the constitutive model in order to represent the linear strain rate dependency and the multitude of relaxation times. By combining the n Maxwell elements with the Hooke element introduced in the standard linear solid model to obtain a long term stress response, it results the linear viscoelastic Wiechert model (i.e. generalised Maxwell model) illustrated in Fig. 1.

In the Wiechert model, the strain on each element is the same as the total strain, and the total stress is the sum of the individual stresses. Applying the superposition theorem, the expression of the stress at time $t$ for the Wiechert model is given by:

$$\sigma^{ve}(t) = \left[E_\infty + \sum_{i=1}^{n} E_i^{ve} exp\left(-\frac{t}{\tau_i}\right)\right]\varepsilon_0 \tag{2}$$

where $E_\infty$ is the added Hooke element stiffness, $E_i$ and $\tau_i$ are the Young modulus and the relaxation time of the $i$th Maxwell element, respectively.

To extend this model in the three dimensions and to take the history of the deformation at time $t$ into account, a Boltzmann superposition principle (or integral) is applied by summing stress increments due to the deformation increment $d\varepsilon(\tau)$ at the previous time $\tau$. This leads to a linear relation between the stress and the strain rate:

$$\sigma^{ve}(t) = \int_{-\infty}^{t} R^{ve}(t-\tau) : \frac{d\varepsilon(\tau)}{d\tau}\, d\tau \tag{3}$$

where $R^{ve}$ is the fourth order relaxation tensor expressed in terms of Prony series as:

$$R^{ve}(t) = \mathscr{L}_\infty^{ve} + \sum_{i=1}^{N} \mathscr{L}_i^{ve} exp\left(\frac{-t}{\tau_i}\right) \tag{4}$$

$\mathscr{L}_\infty^{ve}$ is the fourth order long term elastic tensor and $\mathscr{L}_i^{ve}$ the fourth order elastic stiffness tensor of the $i$th Hooke element, defined by:

$$\mathscr{L}_\infty^{ve} = 2G_\infty I_d + K_\infty I \otimes I,\ \mathscr{L}_i^{ve} = 2\,G_i I_d + K_i I \otimes I, \tag{5}$$

with $I_d$ the deviatoric projection tensor such as:

$$I_d = I_s - \frac{1}{3} I \otimes I \tag{6}$$

and with $I_s$ and $I$ the fourth order symmetric identity and second order identity tensors. As in classical elasticity, the bulk and shear long term moduli are defined by:

$$G_\infty = \frac{E_\infty}{2(1+\nu)}, K_\infty = \frac{E_\infty}{3(1-2\nu)} \tag{7}$$

### 2.2. Viscoplasticity

The commonly used viscoplastic approach is the von Mises plasticity model. However, most polymers have a different behaviour in tension, compression, and shear, and present a volume variation in plasticity so the von Mises yield surface is not correct. To take these aspects into account a non-associative flow rule and a pressure dependent criterion need to be assumed. A non symmetrical yield surface is then used to represent the different behaviours under tension, compression, and shear. This yield surface initially proposed by Raghava [23], expressed in terms of the nominal stress $\tilde{\sigma}$, assumes that the plasticity occurs when the first invariant of the stress tensor ($I_1(\tilde{\sigma})$) and the second invariant of the deviatoric stress tensor ($J_2(\tilde{S})$) reach a critical combination described by:

$$f(\tilde{\sigma}, R) = \frac{(\eta-1)I_1(\tilde{\sigma}) + \sqrt{(\eta-1)^2 I_1^2(\tilde{\sigma}) + 12\eta J_2(\tilde{S})}}{2\eta} - \sigma_t - R(\kappa) \tag{8}$$

with $\kappa$, the equivalent plastic strain defined by:

$$\kappa = \sqrt{\frac{2}{3}\varepsilon_p : \varepsilon_p} \tag{9}$$

where $J_2(\tilde{S})$ is the second invariant of the effective deviatoric stress tensor:

$$J_2(\tilde{S}) = \frac{1}{2}\tilde{S} : \tilde{S} \tag{10}$$

and $I_1(\tilde{\sigma})$ is the first invariant of the effective stress tensor given by:

$$I_1 = tr(\tilde{\sigma}) \tag{11}$$

Finally the parameter $\eta$ characterizes the hydrostatic pressure dependency. It is obtained by using the ratio between the yield stress in compression and tension. It corresponds to the usual way to obtain this parameter even if the hydrostatic stress states are close [23]:

$$\eta = \frac{\sigma_y^c}{\sigma_y^t} \tag{12}$$

with $\sigma_y^c$ and $\sigma_y^t$ respectively the yield stress in compression and in tension.

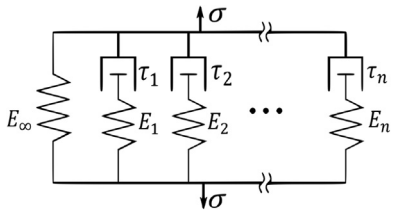


**Fig. 1.** Schema of generalised Maxwell's model.

The behaviour law of the material R(κ) is described by a non-linear isotropic hardening function close to a function already proposed by G'Sell [12].

$$R(\kappa) = Q_1\kappa\, exp(-b_1\kappa) + Q_2(1-exp(-b_2\kappa)) + b_3\kappa^3 + b_4\kappa^2 + b_5\kappa \tag{13}$$

with $Q_1$, $Q_2$, $b_1$ ,$b_2$ ,$b_3$ ,$b_4$ ,$b_5$ the material parameters.

The initial Raghava model is then proposed in its viscoplastic form (Eq. 14) and also with a damage variables on the principle of the effective damage approach to take the growth and nucleation of cavities into account.

$$f(\tilde{\sigma},\kappa,\dot{\kappa},D) = \frac{(\eta-1)I_1(\tilde{\sigma}) + \sqrt{(\eta-1)^2 I_1^2(\tilde{\sigma}) + 12\eta J_2(\tilde{S})}}{2\eta(1-D)} - (\sigma(t) - R(\kappa))\left(\frac{\dot{\kappa}}{\dot{\kappa}_0}\right)^n \tag{14}$$

with $\dot{\kappa}$ the equivalent plastic strain rate, $\dot{\kappa}_0$ the reference plastic strain rate, $n$ a material parameter and where the damage evolution is defined by:

$$D = 1 - exp\left(-\frac{\kappa}{\kappa_c}\right) \tag{15}$$

with $\kappa_c$ a material parameter.

To complete this model and to ensure the volume variation, a second potential is used in the non associated formulation. This potential, close to the first one, is defined by:

$$F^{vp}(\tilde{\sigma}) = \frac{\sqrt{3J_2(\tilde{S}) + \alpha^+ < p >^2 + \alpha^- < -p >^2}}{1-D} \tag{16}$$

with $\alpha^+$ and $\alpha^-$ parameters which define respectively the volume variation for positive and negative hydrostatic pressures.

## 3. Identification of the constitutive model

The material studied is an epoxy adhesive named commercially Sikapower498. The plates of bulk material used for the specimens are obtained by curing the adhesive in a mould under hot press (100 bar) according to polymerisation conditions, i.e. 20 min from 20 °C to 200 °C and then 20 min at 200 °C. The cooling is done at room temperature. The specimens are obtained by water jet cutting from adhesive sheets.

The generalised Maxwell (Eq. 2) parameters are identified by Dynamic Mechanical Analysis (DMA). Monotonic tensile and compression tests are performed at several loading speeds in order to identify the non isochoric viscoplastic behaviour, strain rate dependency, hydrostatic pressure dependency and damage evolution.

### 3.1. Viscoelastic parameters identification

The viscoelastic properties of the adhesive are identified by DMA. Sinusoidal displacement leading to sinusoidal strain (Eq. 17) is applied with an angular frequency $\omega$ to the specimen. The linear elastic assumption is valid only for small amplitudes of strain $\varepsilon_0$. For viscoelastic polymers a phase lag $\delta$ occurs during tests on the stress response described by Eq. (18). The phase lag is related to viscoelastic properties of the material.

$$\varepsilon(t) = \varepsilon_0 cos(\omega t) = \varepsilon_0 R_e\{exp(i(\omega t))\} \tag{17}$$

$$\sigma(t) = \sigma_0 cos((\omega t) + \delta) = \sigma_0 R_e\{exp(i(\omega t + \delta))\} \tag{18}$$

The complex modulus $E^*$ defined by the ratio of stress and strain is written as a function of the frequency :

$$E^*(i\omega) = \frac{\sigma_0}{\varepsilon_0} exp(i\delta) \tag{19}$$

The complex modulus $E^*$ is decomposed into a real component $E'$ (storage modulus), which represents the elastic response and an imaginary component $E''$ (loss modulus) which represents the viscous response.

$$E^* = E' + iE'' \tag{20}$$

The storage and loss moduli are defined by :

$$E' = \frac{\sigma_0}{\varepsilon_0} cos(\delta) \tag{21}$$

$$E'' = \frac{\sigma_0}{\varepsilon_0} sin(\delta) \tag{22}$$

The DMA tensile tests are performed with an electromagnetic device (INSTRON E3000) on straight specimens with a section of 10 mm × 3 mm. The imposed displacement amplitude is 0.1 mm and the frequency varies from 0.1 Hz to 60 Hz. Each branch of the generalised Maxwell model is defined by a stiffness $E_i$ and a relaxation time $\tau_i$. The relations between the time dependent modulus and the complex modulus are given by:

$$E'(\omega) = E_\infty + \sum_{i=1}^{n} E_i \frac{(\omega\tau_i)^2}{1+(\omega\tau_i)^2} \tag{23}$$

$$E''(\omega) = \sum_{i=1}^{n} E_i \frac{\omega\tau_i}{1+(\omega\tau_i)^2} \tag{24}$$

The parameters $E_i$ and $\tau_i$ are found by minimisation of the gap between measured and predicted values of the moduli $E'$ and $E''$, such as:

$$A = \sum_{j=1}^{M} \left[(E'(\omega_j) - E'_m(\omega_j))^2 + (E''(\omega_j) - E''_m(\omega_j))^2\right] \tag{25}$$

where $E'$, $E''$ are calculated from Eq. (23) and Eq. (24) and $E'_m$,$E''_m$ are measured data at $M$ frequency $\omega_j$.

Seven branchs are used to represent the evolution of the complex modulus $E^*$. This number of branchs is fixed as a minimum to satisfy the optimisation criterion and then well describe the viscoelastic behaviour. Table 1 summarizes the set of parameters obtained from model identification given by Eq. (25). The comparisons between the model response and the experimental data are shown in Fig. 2.

### 3.2. Non-isochoric viscoplastic parameters identification

Monotonic uni-axial tensile tests are carried out in order to identify the non-isochoric viscoplastic behaviour of the adhesive. Static tensile tests are performed with an electromagnetic device (INSTRON E3000) on normalised specimens (Fig. 3a) at 1 mm/min and dynamic tensile tests with a hydraulic device (INSTRON VHC) on

**Table 1**
Viscoelastic parameters.

| | $E_i$ [Mpa] | $\tau_i$ [] |
|---|---|---|
| $i=1$ | 262.1 | 100 |
| $i=2$ | 125.4 | 17.78 |
| $i=3$ | 118.02 | 3.1623 |
| $i=4$ | 83.9 | 0.5623 |
| $i=5$ | 66.4 | 0.1 |
| $i=6$ | 44.8 | 0.0178 |
| $i=7$ | 40.445 | 0.0032 |
| $E_\infty$ [MPa] | 1411.6 | |

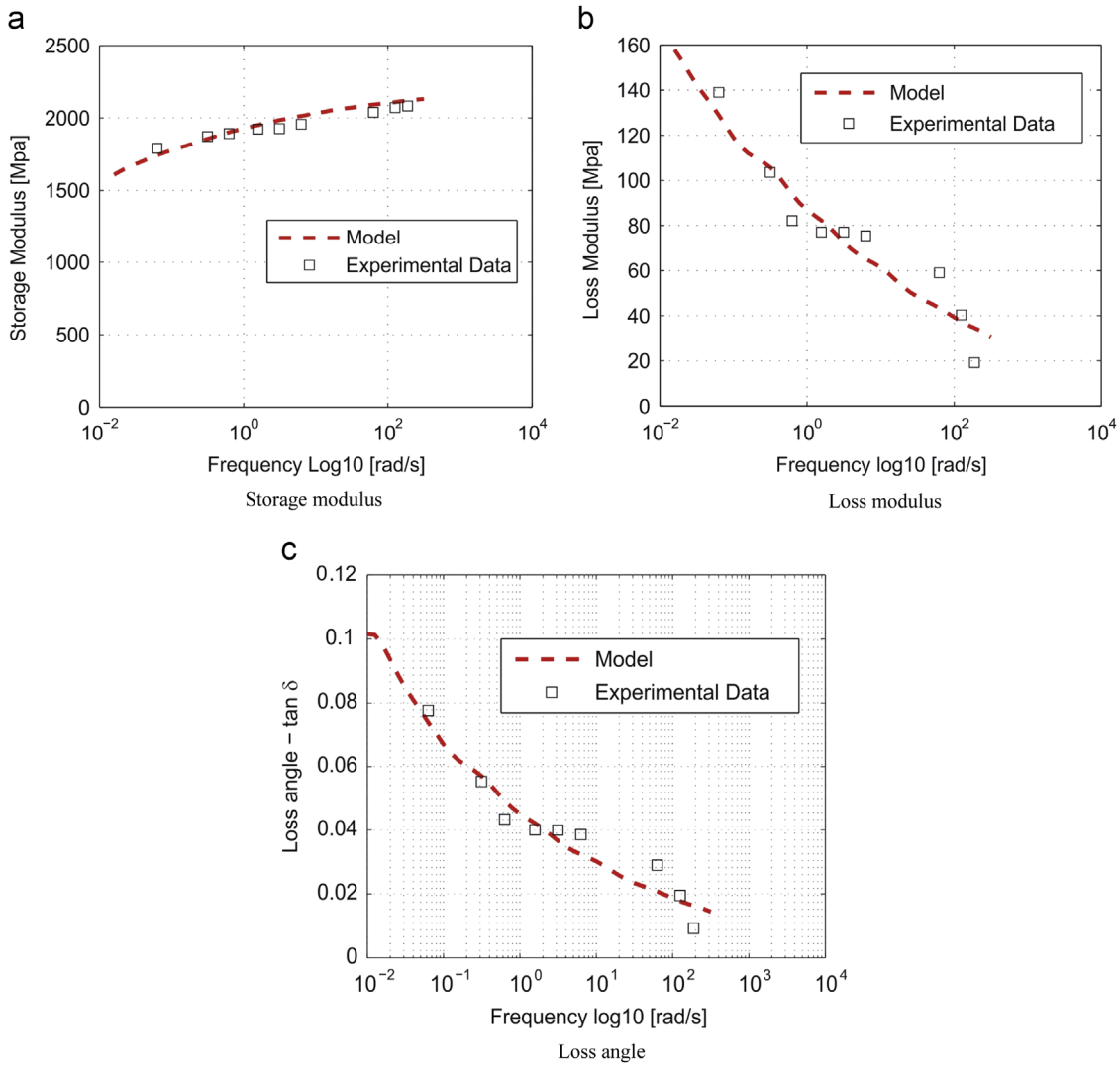


**Fig. 2.** Comparison between viscoelastic model and experimental data.

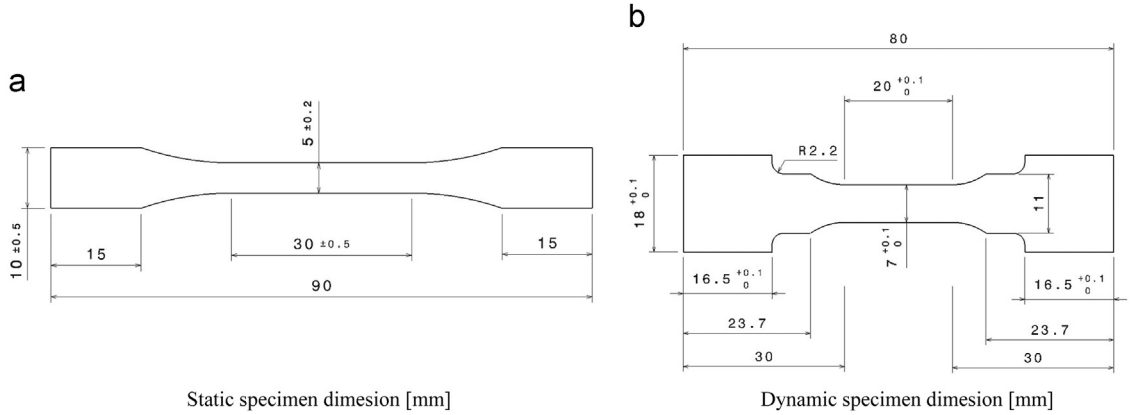


**Fig. 3.** Test specimens.

specific specimens (Fig. 3b) at 10 mm/s, 100 mm/s, and 1000mm/s. Because of thickness variation of bulk specimens, special care is taken on the measurement of the initial section area. In order to avoid as much as possible errors in the computation of the stress. The initial section area used for the computation is the average of 3 sections area measured along the specimen. The variation is less than 2% between the maximum and minimum section areas. Displacements obtained by DIC are used to calculate the deformation of the specimen on a Region of Interest (ROI). The quasi-static tests are performed with two cameras, one in front of the specimen and one in the thickness in order to study the volume variation. For dynamic tests, a single high speed camera (PHOTRON APX 3000) is used in

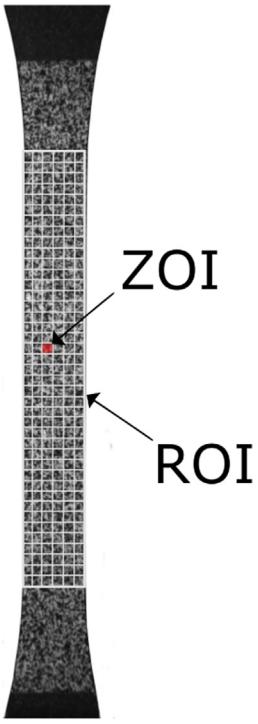


**Fig. 4.** Definition of ZOI and ROI for the strain field measurement by DIC.

front of the specimen. The post-processing by DIC is done with VIC-2D © software. Following Notta-Cuvier and al [20], rigid body motions are used to make sure that the error made on the strain measurement is below 0.01%.

A heterogeneous strain field is generally observed on tensile specimens for polymers due to the appearance of an early necking. This leads to the impossibility to obtain correct behaviour laws at constant strain rate by using classical mechanical analysis. To overcome this issue, *SEÈ* method introduced in [17] is performed. For each test, the DIC allows to compute in each Zone Of Interest (ZOI) of the Region Of Interest (ROI) the true strain and the true strain rate (Fig. 4). The true stress is then obtained by using the incompressible hypothesis according to the equation:

$$\sigma_{yy}^{inc} = \frac{F}{S_0} e^{(\varepsilon_{yy})} \tag{26}$$

Then, a behaviour surface can be built in the space of true equivalent plastic strain, true equivalent strain rate, and true stress (Fig. 5). The data were obtained with different ZOI sizes. It was verified that all ZOI sizes results were in agreement (and no differences are observed according to these different scale analyses).

By cutting this surface at a specific strain rate, the behaviour is achieved at constant strain rate. From this surface, the hardening constitutive model (Eq. 13) is identified. Note that with this hypothesis, the strain rate history of the polymer material is not taken into account. The hardening parameters $Q_1, Q_2$, $b_1$, $b_2$, $b_3$, $b_4$ and $b_5$, and the strain rate parameter $n$, are identified by minimisation using a least squares algorithm. Fig. 9 shows the surface of the hardening law and the parameters are summarised in Table 1. Fig. 6 shows the hardening at 0.12 $s^{-1}$, 2 $s^{-1}$, 21 $s^{-1}$ laws obtained with this methodology.

In order to identify the hydrostatic dependency parameter $\eta$, a compression test at 0.08 mm/min is performed with electromagnetic device on cylinder specimens (⌀=5 mm) The speed is imposed in order to load the compression specimen at the same strain rate as the quasi-static tensile test at 1mm/min. Because of the small size of the specimen, DIC or optical measurement is

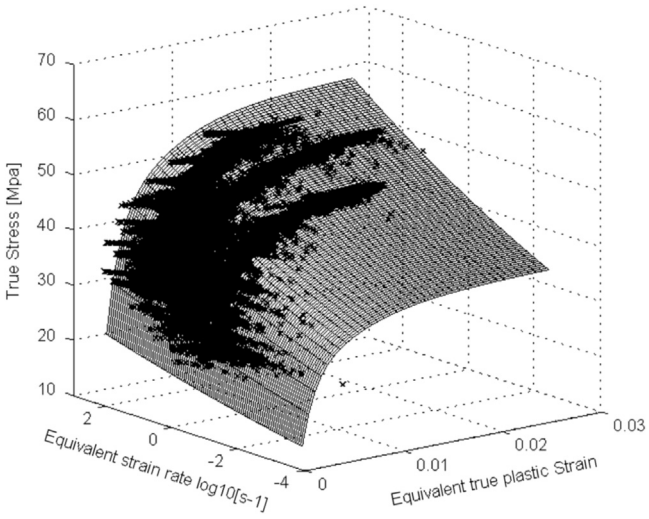


**Fig. 5.** *SEÈ* surface.

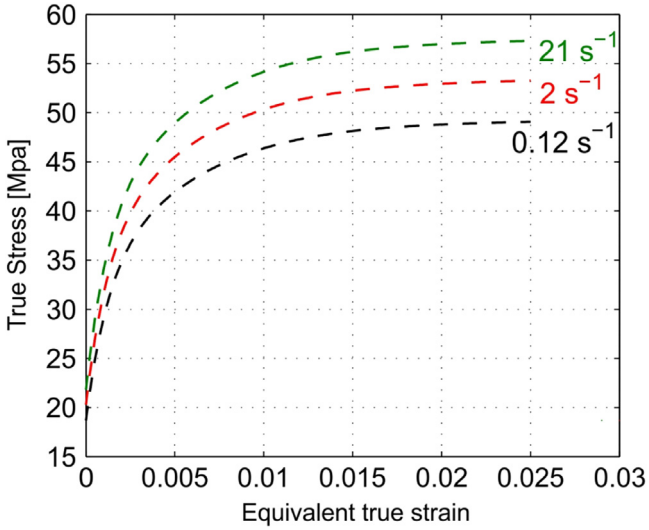


**Fig. 6.** Behaviour law at different strain rates.

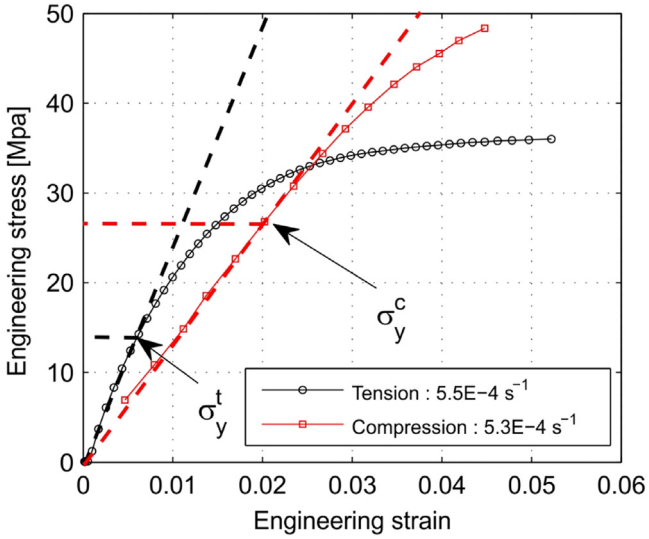


**Fig. 7.** Tension and compression yield stresses.

impossible. The displacement is then obtained directly from the displacement of the compression plates. Fig. 7 shows the difference between tension and compression behaviours. The hydrostatic dependency parameter $\eta$ is identified according to Eq. (12). The yield stresses in tension and compression are identified when the behaviour becomes non linear. The inelastic deformation is considered as viscoplasticity in this work since the permanent strain obtained after a tensile test, is still observed after half an hour release of the stress.

The non-associated flow rule is used to take non-isochoric deformation into account. The viscoplastic dissipation potential is described in Eq. (16) in order to represent the volume change. The parameter $\alpha^+$ represents the dilatation and the parameter $\alpha^-$ the compaction. These parameters are expressed in function of the plastic poisson ratio for positive pressure $\nu_p^+$ and for negative pressure $\nu_p^-$ such as :

$$\alpha^+ = \frac{9}{2}\left(\frac{1-2\nu_p^+}{1+\nu_p^+}\right) \tag{27}$$

$$\alpha^- = \frac{9}{2}\left(\frac{1-2\nu_p^-}{1+\nu_p^-}\right) \tag{28}$$

The plastic Poisson coefficient is a ratio between the transversal and axial plastic strains and is calculated in each ZOI. Fig. 8 shows the evolution of the Poisson coefficient for a quasi static tensile test. The increasing volume of the material is highlighted by the decrease of the Poisson coefficient until approximately 0.3. In compression, the incompressibility hypothesis is used. As a consequence, the parameters take the values $\nu_p^+ = 0.3$ and $\nu_p^- = 0.5$.

As observed in [24], microtomography performed on bulk specimen (Fig. 9) reveals few particles (around 3,5% in volume) with a maximum size of 150 µm and also some fibres with a diameter less than 10 µm and a length around 200 µm. All these inclusions lead to a nucleation process during deformation and then to damage which then reduce the cross section area of the specimen. This damage is then related to the volume/section area variation. It is identified by using the ratio between the compressible (by assuming isotropic transverse behaviour (Eq. 29)) and incompressible stresses (Eq. 26) [13] calculated directly from the data obtained in each ZOI by DIC:

$$\sigma_{yy}^{comp} = \frac{F}{S_0}.e^{(-2\varepsilon_{xx})} \tag{29}$$

where $S_0$ and $\varepsilon_{xx}$ are respectively, the initial cross section and the longitudinal strain calculated in each ROI.

Fig. 10 shows the damage evolution on each ZOI of bulk specimen during the deformation at various loading rates. A scattering of the damage result is observed and it is significant when compared to the value of the damage itself (2%). However, a significant damage evolution can be seen for the cloud of points for the three different speed tests. For each speed loading the evolution is identified. In this case, it is conclude that there is no dependency of the damage evolution model $k_c$ to the loading rate.

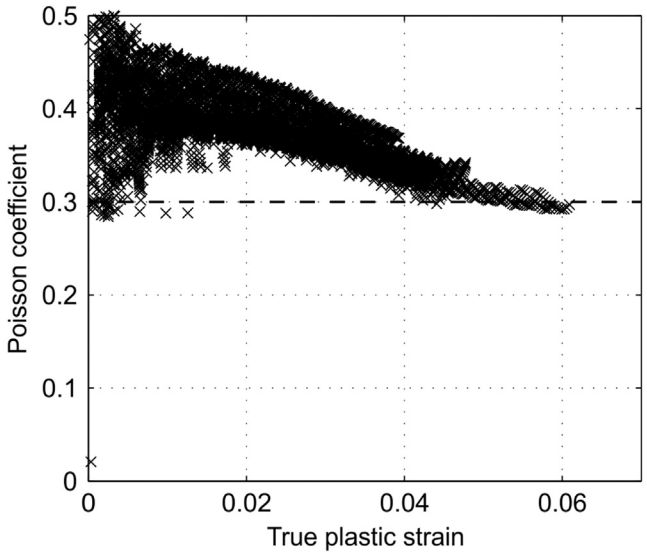


**Fig. 8.** Poisson coefficient for each ZOI.

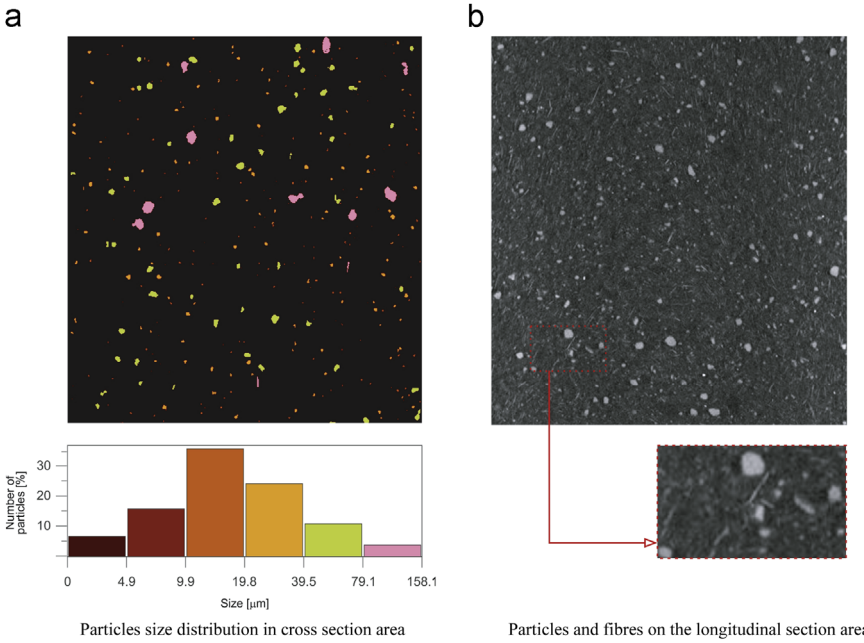


**Fig. 9.** Microtomographic scan of the bulk specimen.

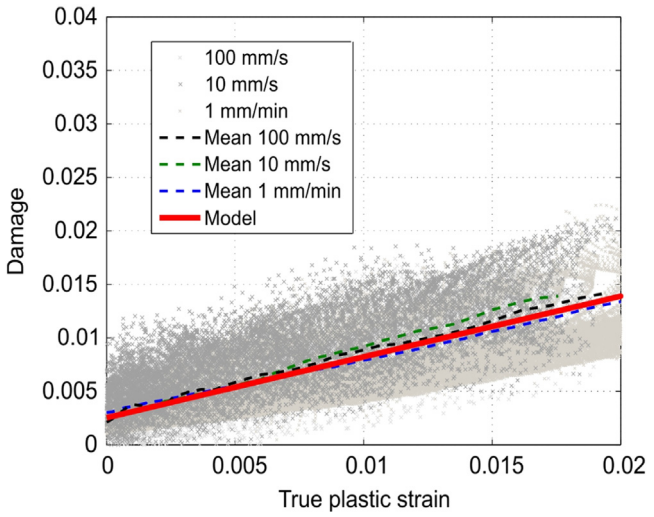


**Fig. 10.** Damage evolution at various loading rates.

**Table 2**
Material parameters.

| | Parameter | Value |
|---|---|---|
| Hardening | $\sigma_t$ [Mpa] | 12 |
| | $Q_1$ | 4000 |
| | $Q_2$ | 15.8 |
| | $b_1$ | 550 |
| | $b_2$ | 240 |
| | $b_3$ | 2.22e-14 |
| | $b_4$ | 2.22e-14 |
| | $b_5$ | 15 |
| Strain rate | $\dot{\kappa}_0$ [$s^{-1}$] | 1e-6 |
| | $n$ | 0.0435 |
| Viscoplastic flow | $\nu_p^+$ | 0.3 |
| | $\nu_p^-$ | 0.5 |
| Pressure dependency | $\eta$ | 1.8 |
| Damage | $\kappa_c$ | 1.75 |

The damage parameter $k_c$ is then determined by least square identification on the whole cloud of points and represented by the red curve in Fig. 10.

The model parameters are summarised in Table 2.

The constitutive identified model is used with the tensile tests. The finite element mesh of the specimen and the boundary conditions employed are shown in Fig. 11. The thickness is modelled with 2 elements according to mesh convergence as discussed in [2]. Fig. 12 shows the comparison between numerical and experimental results. The comparison is carried out on the reaction force versus the relative displacement. The numerical model is in agreement with the experimental results for all speeds.

## 4. Validation of the constitutive model on thin bonded joint

The model has been identified by tensile and compression tests on bulk material (Section 3). The validation is done on thin bonded joints for different angles of loading. Tests and simulations on adhesive bonded joints through a modified Arcan apparatus are thus carried out.

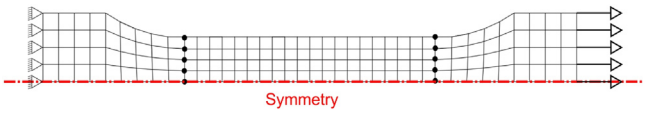


**Fig. 11.** Mesh and boundary conditions for the tensile test simulation.

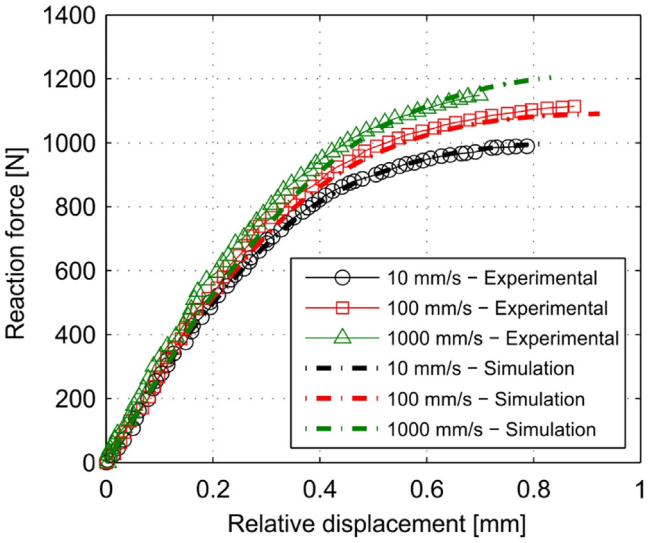


**Fig. 12.** Comparison between experimental and simulation of tensile tests.

### 4.1. Device

Three Arcan devices are designed to load thin bonded joints in pure tensile, shear, and mixed tensile/shear modes (Fig. 13a). The design is based on the modified Arcan fixture developed in [5] for quasi-static loads. The special feature of this new device relies on its low mass required to obtain a noiseless dynamic response, i.e. a force measurement not disturbed by the system resonance. It is composed by two aluminium substrates (AU4G) bonded together with a bonding surface of 10 mm × 40 mm (Fig. 13b). The substrates are considered as to be rigid so as to limit their influence on the mechanical response. Indeed, the stiffness of the substrates is more important than the stiffness of the adhesive.

These substrates are optimised so as to diminish as much as possible the stress singularity at the free edges. The purpose is to avoid failure initiation induced by stress singularity. The design of a beak around the substrate (Fig. 13b) is used according to previous studies performed by ENSTA laboratory [6] in order to minimise the stress singularity. Its geometry is optimised thanks to the simulation of a tensile test. This simulation is based on a plane strain assumption with a fine mesh and a symmetry condition. Ten elements are used to represent the half of the bonded joint (Fig. 14). The substrates are assumed to be elastic ($E$=75 Gpa, $\nu$=0.33). The adhesive is modelled by an viscoelastic–viscoplastic behaviour previously identified. The optimised beak shape leads to local deformations of the substrate which minimise the stress concentrations at the edge of the joint and allow a homogeneous stress distribution in the mean plane of the adhesive as highlighted in (Fig. 15). The von Mises stress is normalised according to the von Mises stress in the centre of the bonded joint in the mean plane.

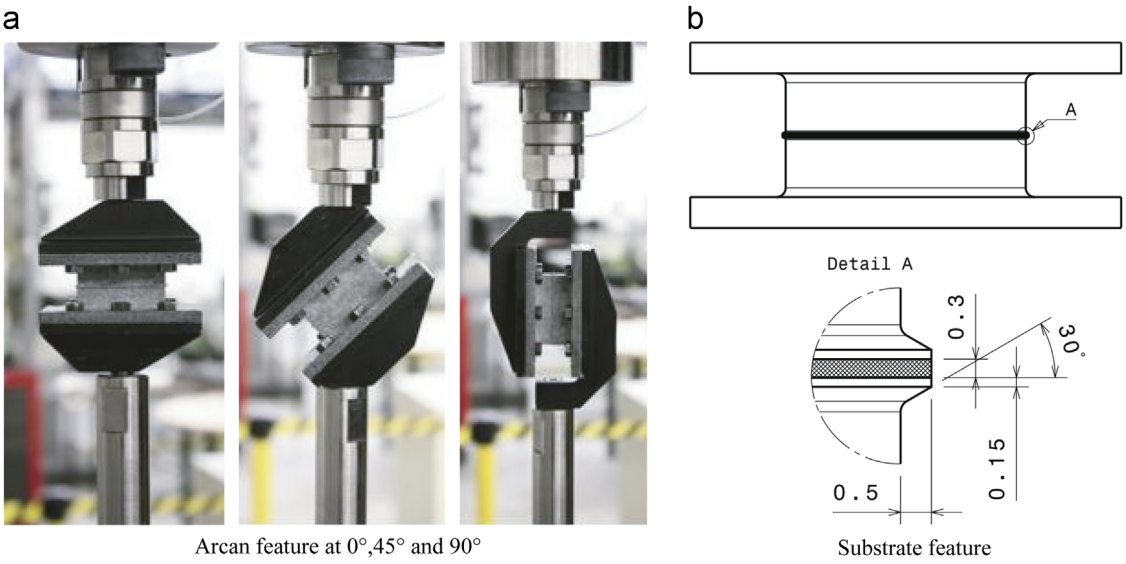


**Fig. 13.** Substrate representation and detail of peak geometry.

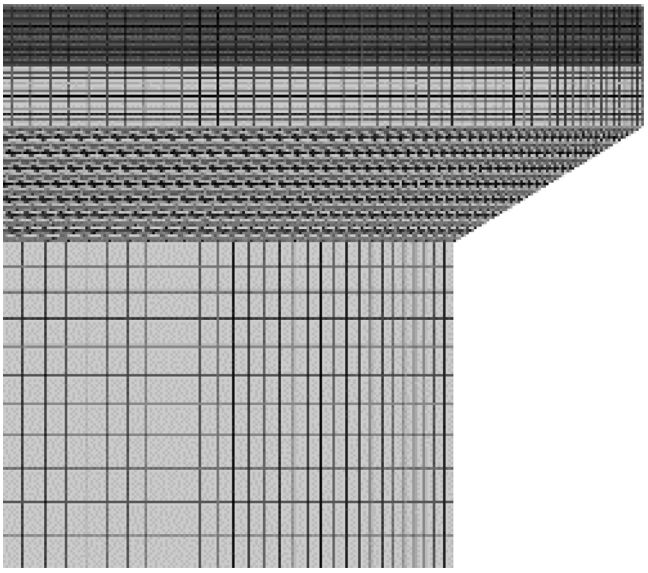

**Fig. 14.** Mesh for the modelling of the beak.

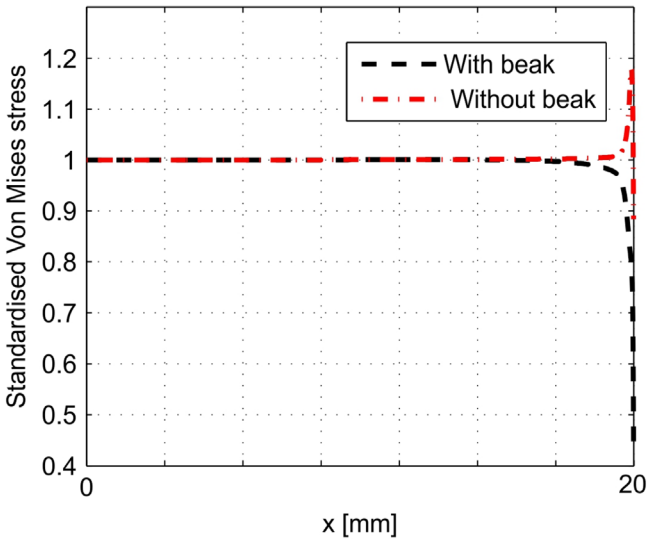


**Fig. 15.** Stress distribution along the joint from the centre ($x=0$) to the beak ($x=20$).

### 4.2. Experimental procedure

For the bonding process, a specific device is designed to assemble substrates with a good adhesive thickness control. After polymerisation, the thickness is checked with a calibrated binocular microscope. For all the specimens, a 0.3 mm ( $\pm$ 0.05 mm) thickness is obtained. The polymerisation conditions are the same as that for bulk material.

The experiments are performed with a dynamic tensile machine INSTRON VHS with imposed load velocity of 1 mm/s, 10 mm/s and 100 mm/s for 0°, 45°, and 90° angles. The force is measured by a KISTLER 30 KN uniaxial piezoelectric load cell, and the relative displacement of the substrates is measured with non-contact measurement technique by DIC. The special pattern needed for the DIC is applied on the substrate with white and black paints (Fig. 17).

### 4.3. Analysis and results

In all tests, cohesive failure is observed (Fig. 16). The images used for DIC are captured with high speed cameras and post-processed with VIC-2D© software in order to measure the relative displacement of the substrates along *Y*-axis (loading direction) and *X*-axis. Two lines are defined below the screw in order to have the same measurement for each test (Fig. 17). The relative displacement is computed as :

$$\delta_X = \frac{\sum_{i=1}^{n}\left[\delta^i_{X_{L1}} - \delta^i_{X_{L2}}\right]}{n} \tag{30}$$

$$\delta_Y = \frac{\sum_{i=1}^{n}\left[\delta^i_{X_{L1}} - \delta^i_{Y_{L2}}\right]}{n} \tag{31}$$

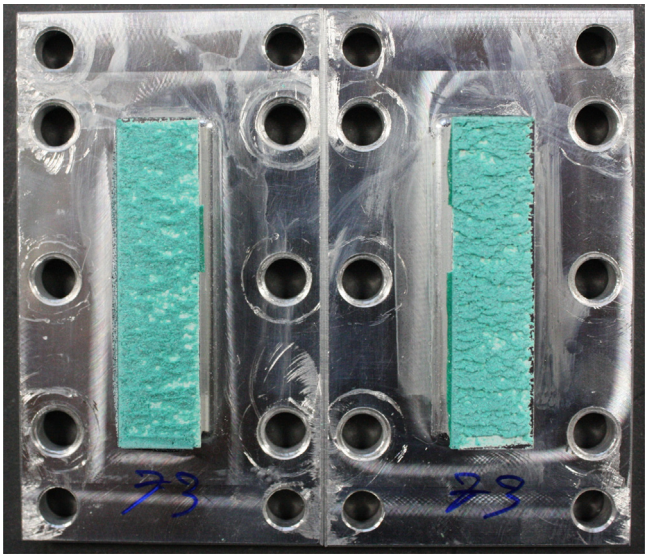

**Fig. 16.** Fracture surface of the Arcan specimen.

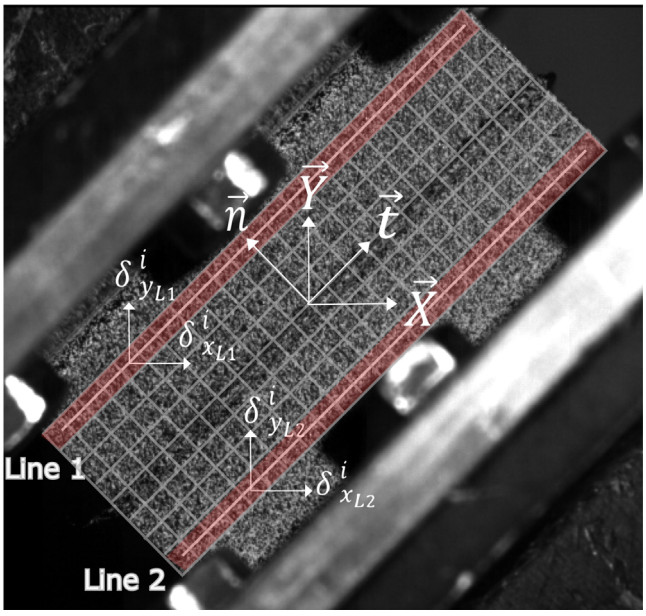


**Fig. 17.** DIC post-processing.

$\delta_X$ and $\delta_Y$ denote the opening and sliding displacements of the joint. $\delta^i_{X_{L1}}$ and $\delta^i_{Y_{L1}}$ are the displacements of the $i^{th}$ ZOI for the line 1 along $X$ and $Y$ axis, $\delta^i_{X_{L2}}$ and $\delta^i_{Y_{L2}}$ are the displacements of the $i$th ZOI for the line 2 along $X$ and $Y$ axis.

The experimental results are presented in Fig. 19. A good repeatability is observed on most of the tests. Only a scattering for the failure displacements is noticed.

### 4.4. Numerical simulation of Arcan tests

Numerical Arcan tests are performed in this section in order to validate the constitutive model described in the previous section. To limit the computation times, only the substrate and the adhesive are taken into account. It can be noticed that the mass of the apparatus is not represented correctly. However, no influence on the result is observed when the total mass of the apparatus is taken into account.

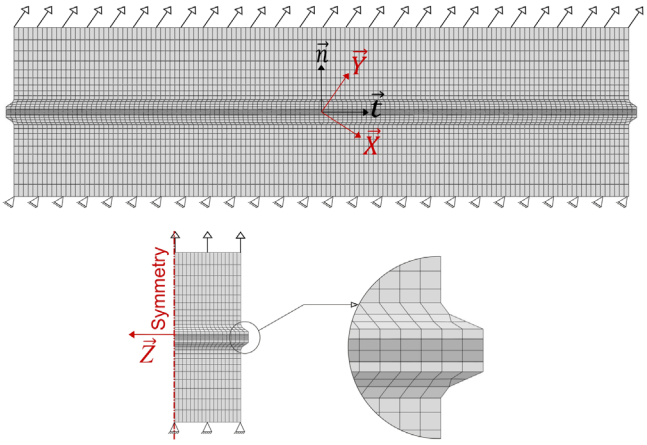


**Fig. 18.** Finite element mesh and boundary conditions.

The substrate and the adhesive are meshed with reduced integration quadratic elements. No real sensitivity of the number of element, through the thickness of the adhesive is observed, so only two elements are used for the present computation. The mesh and the boundary conditions are shown in Fig. 18.

The experimentally measured relative displacement is imposed on the upper substrate along to Y-axis. The bottom face of the top substrate is clamped.

The comparison of the numerical and experimental results are shown in Fig. 19 in terms of relative displacement versus strength. Five tests have been performed for each configuration. The results have highlighted a low scattering under dynamic loading conditions. Thus, only two experimental curves over five have been plotted for conciseness. The results highlight an excellent agreement between simulations and experiments. A little gap is nevertheless observed for the Arcan 45° specimen around the bend of the curve. This gap could be due to the shape of the yield surface which is only determined by tension and compression tests. The model proposed and the identification process associated lead to a good prediction of the adhesive SikaPower498 behaviour under various stress states and with different strain rates.

## 5. Conclusion

A constitutive model initially developed for semi-crystalline polymers is identified in order to model the behaviour of epoxy adhesive. This model based on a viscoelastic–viscoplastic formulation allows to take the strain rate effect, the pressure dependence, the volume variation by using a non associative plasticity, and the damage evolution into account. The identification process associated to this model is based essentially on experiments on bulk specimens. First, the viscoelastic parameters are identified by Dynamical Mechanical Analysis and secondly, the viscoplastic parameters are identified with tensile tests at different strain rates and by applying a specific method called the *SEÈ* method which is adapted for polymer. From these data, the complete behaviour of the adhesive under multiaxial loadings and for a large range of strain rates is defined.

This model is then validated on the tensile tests of the bulk specimens at different speed loadings from 10 mm/s to 1 m/s. It is also validated on a specific Arcan test device designed to represent the loading conditions on a real part under various stress states. The results obtained confirm the quality of this model to determine the true behaviour of the SikaPower498 adhesive. The next step will be now to determine from this specific Arcan device and

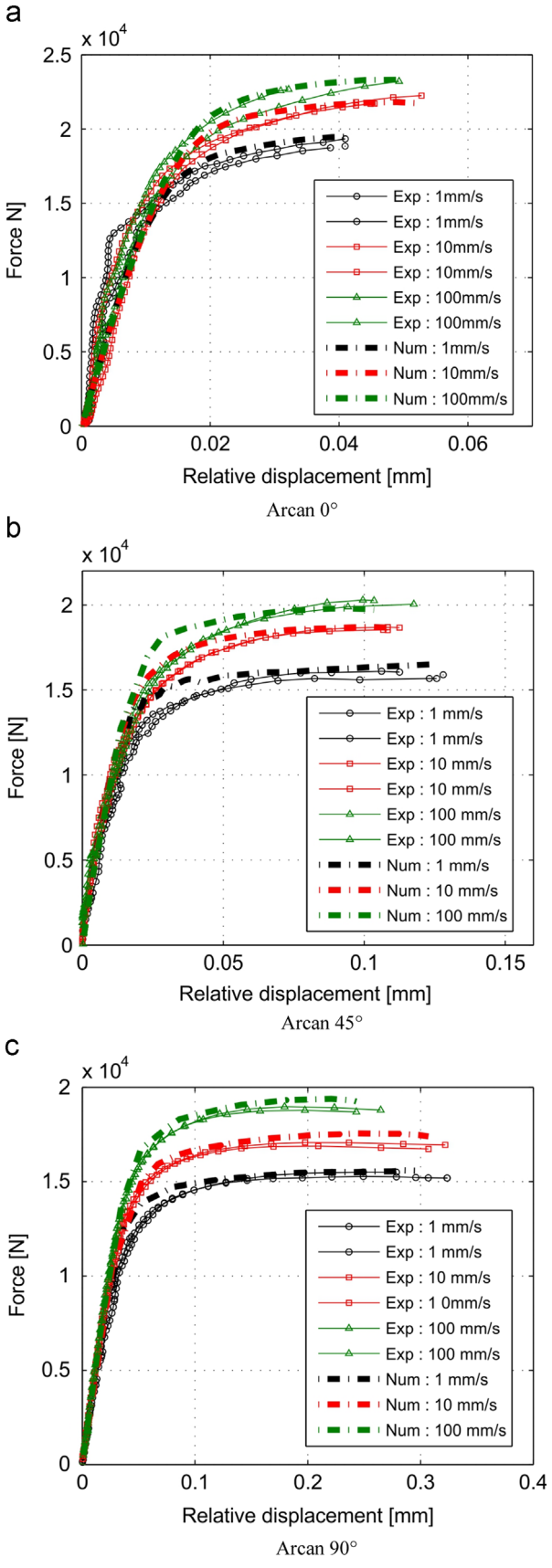


**Fig. 19.** Numerical results for Arcan simulations compared with experiments.

simulations the best failure criteria for different strain rates and for various stress states.

## Acknowledgements

The present research work has been supported by the "Programme véhicule du future" from "Projets d'Investissements d'Avenir" coordinated by ADEME, the International Campus on Safety and Intermodality in Transportation, the "Region Nord Pas de Calais", the European Community, the Delegation Regional of research and technology, the "Ministère de l'Enseignement Supérieur et de la Recherche", and the "Centre National de la Recherche Scientifique": the authors gratefully acknowledge the support of these institutions.

## References

[1] Badulescu C, Germain C, Cognard J, Carrere N. Characterization and modelling of the viscous behaviour of adhesives using the modified arcan device. J Adhes Sci Technol 2015;29(5):443–61.
[2] Balieu R, Lauro F, Bennani B, Delille R, Matsumoto T, Mottola E. A fully coupled elastoviscoplastic damage model at finite strains for mineral filled semi-crystalline polymer. Int J Plast 2013;51(17):241–70.
[3] Balieu R, Lauro F, Bennani B, Matsumoto T, Mottola E. Non-associated visco-plasticity coupled with an integral-type nonlocal damage model for mineral filled semi-crystalline polymers. Comput Struct 2014;134:18–31.
[4] Challita G, Othman R, Khalil K. Compression and shear behavior of epoxy sa 80 bulk adhesive over wide ranges of strain rate. J Polym Eng 2015. http://dx.doi.org/10.1515/polyeng–2015–0062.
[5] Cognard J, Davies P, Gineste B, Sohier L. Development of an improved adhesive test method for composite assembly design. Composites Sci Technol 2005;65(3–4):359–68.
[6] Cognard J. Numerical analysis of edge effects in adhesively-bonded assemblies application to the determination of the adhesive behaviour. Comput Struct 2008;86:1704–17.
[7] Dufour L, Bourel B, Lauro F, Haugou G, Leconte N, Carrere N. A new arcan test device for dynamic loadings of adhesively bonded joints. In: 3rd International Conference on Structural Adhesive Bonding. Porto, Portugal; 2015.
[8] Duncan B, Dean G. Measurement and models for design with modern adhesives. Int J Adhes Adhes 2003;23(2):141–9.
[9] Epee A, Lauro F, Bennani B, Bourel B. Constitutive model for a semi-crystalline polymer under dynamic loading. Int J Solids Struct 2011;48(10):1590–9.
[10] Feucht M, Haufe A, Pietsch G. Adhesive modeling in crash simulation. In: LS-DYNA Forum, Frankenthal. Germany; 2007.
[11] Frank G, Brockman R. A viscoelastic–viscoplastic constitutive model for glassy polymers. Int J Solids Struct 2001;38(30–31):5149–64.
[12] G'Sell C, Jonas J. Determination of the plastic behaviour of solid polymers at constant true strain rate. J Mater Sci 1979;14:583–91.
[13] G'Sell C, Hiver J, Dahoun A. Experimental characterization of deformation damage in solid polymers under tension, and its interrelation with necking. Int J Solids Struct 2002;39:3857–72.
[14] Goda Y, Sawa T. Study on the effect of strain rate of adhesive material on the stress state in adhesive joints. J Adhes 2011;87(7–8):766–79.
[15] Goglio L, Peroni L, Peroni M, Rossetto M. High strain rate compressive and tension behaviour of an epoxy bi–component adhesive. Int J Adhes Adhes 2008;28(7):329–39.
[16] Jousset P, Rachik M. Implementation, identification and validation of an elasto-plastic-damage model for the finite element simulation of structural bonded joints. Int J Adhes Adhes 2014;50:107–18.
[17] Lauro F, Bennani B, Morin D, Epee A. The *SEÈ* method for determination of behavior laws for strain rate dependent material: application to polymer material. Int J Impact Eng 2010;37(6):715–22.
[18] Morin D, Haugou G, Bennani B, Lauro F. Experimental characterization of a toughened epoxy adhesive under a large range of strain rates. J Adhes Sci Technol 2011;25:1581–602.
[19] Morin D, Bourel B, Bennani B, Lauro F, Lesueur D. A new cohesive element for structural bonding modelling under dynamic loading. Int J Impact Eng 2013;53:94–105.
[20] Notta-Cuvier D, Langrand B, Markiewicz E, Lauro F, Portemont G. Identification of johnson-cook's viscoplastic model parameters using the virtual fields method: application to titanium alloy ti6al4v. Int J Exp Mech 2013;49(1):22–45.

[21] Pandey P, Shankaragouda H, Singh AK. Nonlinear analysis of adhesively bonded lap joints considering viscoplasticity in adhesives. Comput Struct 1999;70(4):387–413.
[22] Rabinowitz S, Ward I, Parry J. The effect of hydrostatic pressure on the shear yield behaviour of polymers. J Mater Sci 1970;5(1):29–39.
[23] Raghava R, Cadell RM, Yeh GSY. The macroscopic yield behaviour of polymers. J Mater Sci 1973;8(2):225–32.
[24] Stamoulis G, Carrere N, Cognard J, Davies P, Badulescu C. On the experimental mixed-mode failure of adhesively bonded metallic joints. Int J Adhes Adhes 2014;51:148–58.
[25] Taib A, Boukhili R, Achiou S. Bonded joints with composite adherends. part ii. finite element analysis of joggle lap joints. Int J Adhes Adhes 2006;26(4):237–48.
[26] Tvergaard V, Hutchinson J. The relation between crack growth resistance and fracture process parameters in elastic-plastic solids. J Mech Phys Solids 1992;40(6):1377–97.